Accepted Manuscript

Study of the binding way between saxitoxin and its aptamer and a fluorescent aptasensor for detection of saxitoxin

Sheng Cheng, Bin Zheng, Dongbao Yao, Shenglong Kuai, Jingjing Tian, Haojun Liang, Yunsheng Ding

PII:	S1386-1425(18)30570-5
DOI:	doi:10.1016/j.saa.2018.06.036
Reference:	SAA 16195
To appear in:	*Spectrochimica Acta Part A: Molecular and Biomolecular Spectroscopy*
Received date:	31 March 2018
Revised date:	7 June 2018
Accepted date:	10 June 2018

Please cite this article as: Sheng Cheng, Bin Zheng, Dongbao Yao, Shenglong Kuai, Jingjing Tian, Haojun Liang, Yunsheng Ding , Study of the binding way between saxitoxin and its aptamer and a fluorescent aptasensor for detection of saxitoxin. Saa (2017), doi:10.1016/j.saa.2018.06.036

Study of the binding way between saxitoxin and its aptamer and a fluorescent aptasensor for detection of saxitoxin

Sheng Cheng[1], Bin Zheng[2,], Dongbao Yao[3], Shenglong Kuai[4], Jingjing Tian[1], Haojun Liang[3], Yunsheng Ding[1,*]*

1. Department of Polymer Science and Engineering, School of Chemistry and Chemical Engineering, Anhui Key Laboratory of Advanced Functional Materials and Devices, Hefei University of Technology, Hefei, Anhui 230009, P.R. China

2. School of Chemistry and Chemical Engineering, Hefei Normal University, Hefei, Anhui 230061, P.R. China

3. Department of Polymer Science and Engineering, University of Science and Technology of China, Hefei, Anhui 230026, P.R. China

4. Anhui Technical College of Water Resources and Hydroelectric Power, Hefei, Anhui 231603, P.R. China

* To whom correspondence should be addressed.

Dr. Bin Zheng

Email: paradise@mail.ustc.edu.cn Tel: 86-551-63758370

School of Chemistry and Chemical Engineering, Hefei Normal University

Prof. Yunsheng Ding

Email: dingys@hfut.edu.cn Tel: 86-551-62901545

Department of Polymer Science and Engineering, School of Chemistry and Chemical Engineering, Anhui Key Laboratory of Advanced Functional Materials and Devices, Hefei University of Technology

Abstract

Aptamers could be used to construct simple and effective biosensor because the conformational switch of aptamer upon target binding is easy to be transferred to optical or electrochemical signals. Nevertheless, we found that the binding between saxitoxin (STX) and aptamer (M-30f) is not accompanied with conformational switch. Here, the circular dichroism spectra, fluorophore and quencher labeled aptamer, and crystal violet-based assays were used to identify the binding way between STX and aptamer. The results show that the conformation of aptamer is stabilized in PBS buffer (10 mM phosphate buffer, 2.7 mM KCl, 137 mM NaCl, pH 7.4) and this conformation may provide an exactly suitable cave for STX binding. Through the analysis of UV-melting curves and circular dichroism-melting curves, it is found that different concentrations of STX produce different unfolding extents of the aptamer under high temperature. Then, a simple temperature-assisted "turn-on" fluorescent aptasensor was developed to detect STX and the application in real sample detection demonstrates its feasibility. The proposed method provides not only an alternative for STX detection but also a strategy for simple aptasensor design using aptamers that do not switch conformation upon targets binding.

Keywords: biosensor; aptamer; binding way; saxitoxin; paralytic shellfish toxin

Introduction

Saxitoxin (STX), a mostly studied paralytic shellfish toxin, is produced by cyanobacteria and dinoflagellates [1]. It can be accumulated by filter-feeding bivalves and fish, and thus enter the food chain. Its toxicity comes from its binding with the voltage gated sodium channel and subsequently blocking the passage of nerve impulses [2]. The exposure to STX could lead to paralysis, respiratory failure, and even death [3, 4]. Considering the food safety and environmental sustainability, a worldwide regulatory limits for paralytic shellfish toxin have been set to be 80 μg STX eq./100 g shellfish [1, 5, 6]. Thus, the rapid detection of STX is required because of its threat to human health. Up to now, several techniques have been developed in the detection of STX.

The mouse bioassay is an internationally accredited Association of Analytical Communities (AOAC) method that can provide adequate accurate results for STX detection (Mouse bioassay 959.08) [7]. However, it is not suitable for onsite application. The criticism for ethical issues, poor specificity, low sensitivity and the need of a large number of live animals limit its application [2, 8, 9]. High performance liquid chromatography (HPLC) and its coupled techniques have the advantages of sample separation and quantification with high sensitivity, which has been an important technique in STX detection, such as LC-fluorescence detection [10-12]. However, the preparation and analysis of samples are time-consuming, and it needs sophisticated technicians, expensive instruments and toxin standards [2, 9]. Some other techniques, such as surface enhanced Raman scattering (SERS) [13] and the synthesis of chemosensors [14] have also been proposed. They are simple but the problem of specificity has to be overcome. Therefore, more simple and rapid monitoring methods are urgently required.

Biosensors are more effective, commonly sensitive and specific methods in analytes detection

[15]. The immunosensors based on surface plasmon resonance, fluorescence and electrochemistry have been applied in the detection of STX [16-18]. However, the use of antibodies as molecular recognition elements has some drawbacks, such as high production costs and cross reactivity, special storage and operation requirements, and the use of experimental animals [19]. Aptamers are single-stranded DNAs or RNAs that have a high affinity to a specific target molecule [20, 21]. Compared with antibodies, aptamers possess the advantages of high specificity and binding affinity, high chemical stability, easy synthesis and modification [19, 22]. Therefore, aptamers have been widely applied in biosensors for various targets detection since its first identification in 1990 [23-26] such as food toxin [27]. The DNA aptamer (APT^{STX1}) for STX was first reported in 2013 [28] and a high resolution melting profile-based method was developed to detect STX [29]. Nevertheless, the aptamer strand is too long (78 bases) and the binding affinity is not satisfied (K_d is 3.84 μM). Zhang et al. optimized it by rational site directed mutagenesis and truncation and a shorter aptamer M-30f (34 bases) with higher binding affinity (K_d is 133 nM) was generated in 2015 [30]. Then, a biolayer interferometry competitive biosensor was fabricated through the change in the optical thickness and mass density of the biosensor layer upon STX binding [2].

A conformational switch of aptamer is usually accompanied with the target binding. The behavior of conformational switch is easy to be transferred to other signals for simple aptasensors design. For example, the control of conformational switch to the aggregation of gold nanoparticle has been an excellent colorimetric biosensing method [31]; the conformation switch induced fluorescence resonance energy transfer (FRET) is a simple strategy for fluorescent aptasensor design [22, 32-34]. However, to the best of our knowledge, there was no report on the binding mechanism between STX and M-30f, especially the binding way. The reported work, the biolayer biosensor, could be performed

because that method does not need to consider the conformational switch. Without the clarification of the binding way between STX and M-30f, it is difficult to design effective biosensors for the detection of STX. Here, the circular dichroism spectra and fluorophore and quencher labeled aptamer were used to identify the conformational switch during the binding process. Then, crystal violet, a triphenylmethane dye that selectively binds to the G-quadruplex motif [35, 36], was used to investigate the possible binding mode of STX to the aptamer. Finally, the UV-melting curves analysis of the aptamer-STX complex was studied and a temperature-assist fluorescent aptasensor was developed for the detection of STX.

Materials and methods

Materials

All oligonucleotides (HPLC grade), crystal violet and PBS powder were purchased from Sangon Biotechnology Inc. (Shanghai, China). The oligonucleotides sequences are listed as follows: M-30f (5'-TTG AGG GTC GCA TCC CGT GGA AAC AGG TTC ATT G-3'), fluorophore (HEX, hexachlorofluorescein) and quencher (BHQ1, black-hole quencher 1) labeled aptamer, HB-M-30f (HEX 5'- TTG AGG GTC GCA TCC CGT GGA AAC AGG TTC ATT G-3' BHQ1). DNA solutions were prepared by dissolving these oligonucleotides in water. They were heated to 94 ^{o}C to dissociate any intermolecular interaction followed by quenching in a 0 ^{o}C water bath and their concentrations were determined by measuring their UV absorbance at 260 nm. Extinction coefficients of each nucleotide were: ε(dA) = 15400 M^{-1} cm^{-1}, ε(dG) = 11500 M^{-1} cm^{-1}, ε(dC) = 7400 M^{-1} cm^{-1}, and ε(dT) = 8700 M^{-1} cm^{-1}.

Saxitoxin dihydrochloride (66.3 μM in 3 mM HCl), gonyautoxin-2, and -3 (GTX2&3, 157.6 μM in 3 mM HCl), and neosaxitoxin (NEO, 65.6 μM in 3 mM HCl) were obtained from the National

Research Council Canada (Halifax, NS). PBS buffer used was 10 mM phosphate buffer, 2.7 mM KCl, 137 mM NaCl, pH 7.4. Tris-HCl used was 10 mM Tris-HCl, pH 7.4. All the other reagents (analytical reagent) were purchased from Sinopharm Chemical Reagent Co., Ltd (Shanghai, China), and were used as received. Milli-Q water (18.2 MΩ•cm) (Millpore Co., USA) was used throughout the study.

Circular dichroism (CD) measurements

The CD spectra were collected using a JASCO J-810 spectropolarimeter at 25 °C. The data were collected from 200 nm to 400 nm in a sealed 10 mm path-length quartz cuvette at a scanning rate of 100 nm min^{-1} and presented as an average of three successive scans. The final concentrations of the aptamer were 5 μM both in Tris-HCl and PBS conditions. The mixtures were incubated for 1 h at room temperature before measurements. The scan of the buffer alone under the same conditions was used as the blank, which was subtracted from the average scan of each sample. The cell-holding chamber was flushed with a constant stream of dry nitrogen gas to avoid water condensation on the cell.

CD-melting curves were obtained by monitoring the ellipticity at 297 nm as a function of temperature. The solutions containing 5 μM M-30f, 10 mM PBS and various concentrations of STX were incubated for 1 h at room temperature. Then they were allowed to stand at 25 ºC for 5 mins before being heated to 99 ºC at a heating rate of 1.5 ºC min^{-1} in sealed 10 mm path-length quartz cells. The melting temperature (T_m) values of the complexes were estimated with similar method as that in UV-melting curve.

Fluorescence measurements

All fluorescence measurements were carried out on a HITACHI F-7000 fluorescence spectrophotometer. In the assays that using HEX and BHQ1 labeled aptamer (HB-M-30f) for the analysis of STX-M-30f conformation, the final concentrations of the aptamer were 100 nM both in

Tris-HCl and PBS conditions. The mixtures were incubated for 1 h at room temperature before measurements. The excitation wavelength was 530 nm, and the slit widths for excitation and emission were 5 nm and 5 nm, respectively. In CV assays, the final concentrations of aptamer and CV were 4 μM and 8 μM, respectively. The excitation wavelength was 580 nm, and the slit widths for excitation and emission were 10 nm and 10 nm, respectively.

UV-melting curves

UV-melting curves were obtained by monitoring the UV absorbance at 260 nm as a function of temperature on an Agilent Cary 300 UV-vis spectrophotometer. The solutions containing 1 μM M-30f, 10 mM PBS and various concentrations of STX were incubated for 1 h at room temperature. Then they were allowed to stand at 25 °C for 5 mins before being heated to 99 °C at a heating rate of 1.5 °C min^{-1} in sealed 10 mm path-length quartz cells. The melting temperature (T_m) values of the complexes were calculated by fitting the experimental curves with a Sigma plot, where T_m is the midpoint temperature of the order–disorder transition of the complex [37].

Temperature-assisted biosensing assay

In STX detection assays, 4 μL of HB-M-30f (1 μM), 20 μL of PBS (100 mM) and various volumes of STX (66.3 μM) were mixed together and appropriate volumes of water were added to make a total volume of 200 μL. The mixed solutions were incubated for 0.5 h at room temperature before being transferred into sealed 10 mm path-length quartz cells. These cells were allowed to stand at 61 °C for 10 min in the fluorescence spectrophotometer equipped with a circular water bath before measurements. The excitation wavelength was 530 nm, and the slit widths for excitation and emission were 5 nm and 5 nm, respectively. To determine the selectivity of the biosensing, the assays were repeated with water (blank) and standard solutions of GTX2&3 and NEO.

Detection of STX in real samples

Shellfish samples which were purchased from supermarket were used to assess the feasibility of this fluorescent aptasensor for the detection of STX. The shellfish sample extraction was performed according to the AOAC procedure [2, 38]. Briefly, the shellfish meat was thoroughly cleaned and homogenized in a blender. 5 g of the homogenate were spiked with various volumes of STX standard solutions. The samples were vortex mixed after the addition of 3 mL of 1% acetic acid solution, and then boiled for 5 min. After cooling to room temperature, the mixtures were centrifuged at 5000 rpm for 5 min after a short shake. The supernatant was collected and the residual was extracted twice by repeating the above procedure. The collected supernatant was dried and suspended in 200 μL of PBS buffer. Then, 100 μL of the extracted solution, 4 μL of HB-M-30f (1 μM), and appropriate volumes of PBS buffer and water were added to make a total volume of 200 μL. The mixtures were analyzed using the above temperature-assisted biosensing assay.

Results and Discussion

Analysis of aptamer conformation switch by CD spectra

The conformational switch upon STX binding was studied through the analysis of CD spectra under different conditions. Because the PBS buffer (10 mM phosphate buffer, 2.7 mM KCl, 137 mM NaCl, pH 7.4) is the experimental condition for STX aptamer screening and optimization, the CD spectra of M-30f in PBS conditions are studied firstly (Fig. 1A, Line 1-3). It can be seen that there is no obvious change after the addition of STX. The positive peak at 272 nm and the negative peak at 241 nm represent the formation of B-form duplex [39] which is caused by the stem-loop structures predicted using the mfold web server [30]. Thus, it is found that the conformation has been stabilized before the addition of STX. As this conformation is determined by the buffer conditions and the existence of

G-quadruplex has been predicted in Zheng's work [30] using QGRS Mapper, Tris-HCl buffer was selected to further study the conformation of M-30f because this buffer does not contain metal ions which could induce G-quadruplexes. The CD spectrum of M-30f in Tris-HCl condition is shown in Fig. 1A (Line 5). It is found that the duplex still exists in the conformation under Tris-HCl conditions and the difference is that the absorbance increases at around 300 nm in PBS buffer which may be caused by the formation of G-quadruplex. What is more, the PBS buffer used in this work contains 2.7 mM K^+ which is an effective G-quadruplex stabilizer and the significance of K^+ in this system has been studied by Gao [2]. Thus, K^+ was also added into Tris-HCl buffer and the same phenomenon appeared (Fig. 1A, Line 4). Then, the data process was performed by subtracting Line 5 from Line 1-4 and the results are shown in Fig. 1B. In the subtracted spectra, an obvious positive peak appears at around 297 nm and a negative peak appears at around 269 nm which suggests the existence of G-quadruplex structures [39].

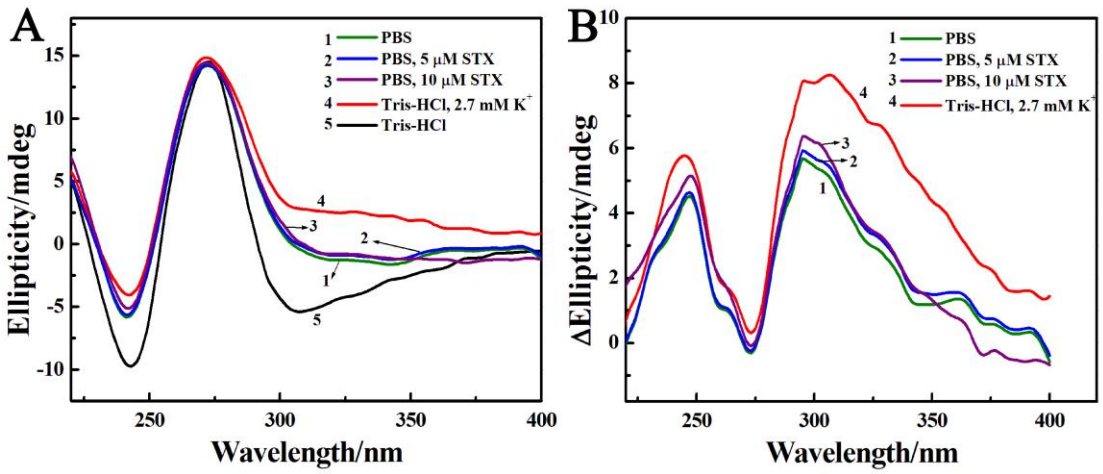

Fig. 1 (A) CD spectra of M-30f (5 μM) under various buffer conditions: 1) PBS buffer (10 mM phosphate buffer, 2.7 mM KCl, 137 mM NaCl, pH 7.4), 2) the addition of 5 μM STX under PBS condition, 3) the addition of 10 μM STX under PBS condition, 4) Tris-HCl buffer (10 mM Tris-HCl, pH 7.4) with 2.7 mM KCl, and 5) Tris-HCl buffer; (B) The obtained CD spectra by subtracting Line 5 from Line 1-4 in (A).

Analysis of aptamer conformation switch by FRET

To further clarify the conformational switch process, fluorescence resonance energy transfer (FRET) is employed here to study the distance change between two termini of the M-30f strand using the labeled aptamer strand (HB-M-30f) which contains the fluorophore HEX and the quencher BHQ1 at its 5' and 3' termini, respectively. The labeled sites were selected at termini because it could avoid the interference from fluorophore or quencher to the binding between STX and aptamer. The extent of FRET is strongly depended on the distance between the donor and acceptor. The conformational switch might induce the distance change between two termini and hence change the fluorescent intensity of the solution. It can be seen from Fig. 2 that the solution of HB-M-30f emits a strong fluorescence at 553 nm under Tris-HCl condition (without K^+) while the fluorescent intensity decreases greatly under PBS conditions demonstrating the occurrence of a conformational switch. This is coincident with the conclusion of CD analysis. The formation of G-quadruplex structure under PBS condition brings the fluorophore and the quencher in close proximity to form a more compact structure, and thus FRET occurs. What is more, the addition of STX with different concentrations does not produce obvious change both in Tris-HCl buffer and PBS buffer. To exclude the possibility of phosphate effect on the fluorescence decrease of HEX, the fluorescence spectrum of HB-M-30f in pure PBS buffer (10 mM phosphate buffer) was collected which is shown in Fig. 2A (dotted line). It can be seen that the fluorescence was recovered to similar level with that in Tri-HCl buffer suggesting that the phosphate buffer has less effect on fluorescence decrease. To demonstrate the effect of K^+, the fluorescence spectrum of HB-M-30f in pure PBS buffer containing different concentrations of K^+ were investigated (Fig. 2B). A sharp decrease of fluorescence intensity occurred after the addition of K^+ indicating the folding of aptamer, and the decrease rate tends to slow down after 3 mM of K^+. The intensity at 553 nm

of pure PBS buffer containing 2.7 mM K^+ from Fig. 2B (inset) can be estimated to be 4100 which is similar to that in aptamer screening PBS buffer (3970) (Fig. 2A, PBS series) which also contains 2.7 mM of K^+. These results demonstrate that the decrease of fluorescence intensity in PBS buffer is mainly attributed to K^+.

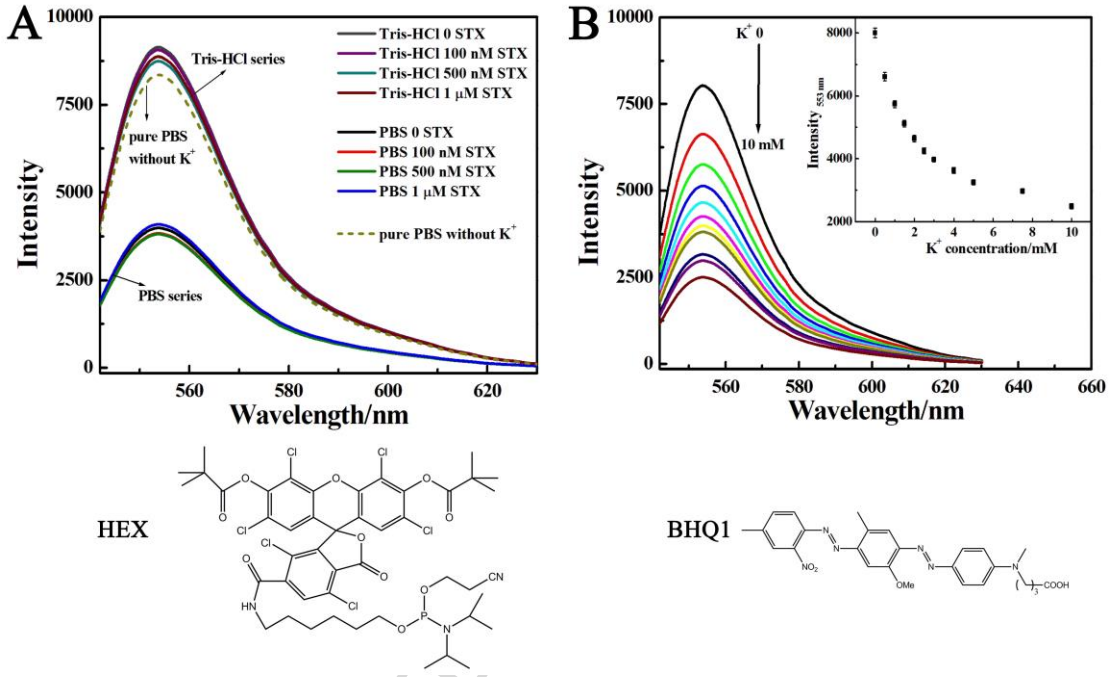

Fig. 2 (A) Fluorescence spectra of HB-M-30f (100 nM) in the presence of various concentrations of STX in PBS buffer and Tris-HCl buffer (solid lines), and fluorescence spectrum of HB-M-30f (100 nM) in pure PBS buffer (dotted line). (B) Fluorescence spectra of HB-M-30f (100 nM) in the presence of various concentrations of K^+ in pure PBS buffer. The inset is the fluorescence intensity at 553 nm as function of concentration of K^+. The chemical structures of HEX and BHQ1 are shown at the bottom of this figure.

Thus, we infer that the presence of STX cannot change the conformation of aptamer alone. There might be some interactions between STX and random aptamer but it is not strong enough to dominate the conformation of aptamer. The buffer condition, especially K^+, is the main factor to determine its final conformation. As this aptamer was developed in the PBS solution (10 mM phosphate buffer, 2.7

mM KCl, 137 mM NaCl, pH 7.4), only the final conformation formed under such condition has the ability to recognize STX, such as some special sites involved for STX binding. Consequently, a brief conclusion could be obtained that the conformation of the aptamer (M-30f) does not change upon STX binding under the PBS conditions and the formation of G-quadruplex plays an important role for STX binding.

CV-based fluorescent assay

As the formation of G-quadruplex structure makes the aptamer has the ability to bind STX, we hypothesize if STX was stacked onto or surrounded by this structure. CV is a commercially available, fluorescent, triphenylmethane dye that binds selectively to the G-quadruplex motif through the external stacking mode [35, 36]. The fluorescence of free CV is weak, while it could be enhanced significantly after binding with G-quadruplex. Therefore, if STX is stacked onto G-quadruplex, the addition of STX could decrease the fluorescence intensity because the binding affinity between STX and M-30f (K_a is 7.5 μM^{-1}) is much higher than that between CV and G-quadruplex (K_a is 0.05 μM^{-1} or less). As is shown in Fig. 3, the fluorescence of CV is enhanced after the addition of M-30f. However, the addition of STX could not decrease the fluorescence intensity which indicates that the binding site between STX and aptamer does not adopt the external stacking mode. We infer that the formation of duplex and G-quadruplex structure may provide an exactly suitable cave for STX binding which is consistent with Zheng's assumption [30].

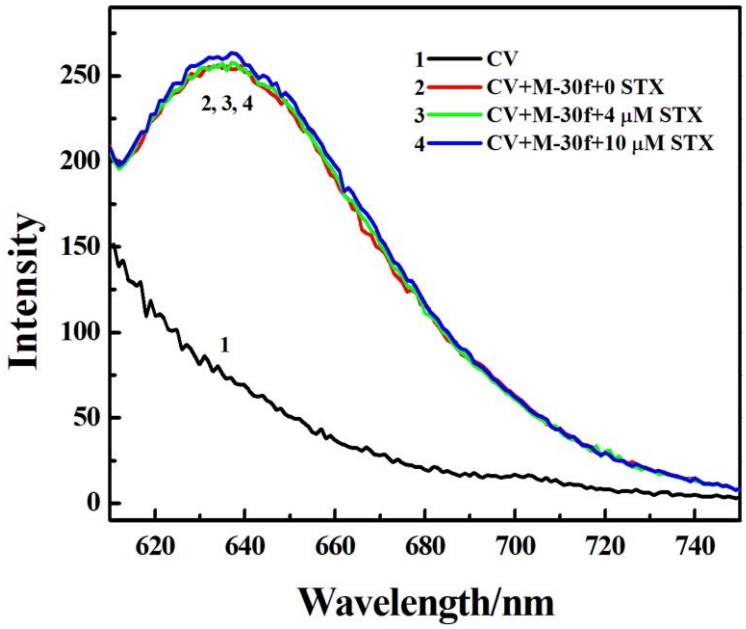

Fig. 3 Fluorescence spectrum of CV (8 μM) (Line 1), and spectra of the mixture of CV (8 μM) and M-30f (4 μM) in the presence of various concentrations of STX (Line 2: 0 STX; Line 3: 4 μM STX; Line 4: 8 μM STX).

Analysis of UV-melting curves and CD-melting curves

The binding between target and aptamer without conformational change is an obstacle for biosensor design. As the binding of STX may alter the thermal stability of the folded structure, we hypothesize that the melting temperature may be altered. With the increase of temperature, the folded structure would be unfolded and expose DNA bases which make the adsorption at 260 nm increase. Fig. 4A shows the UV-melting curves of the aptamer solutions incubated with various concentrations of STX. In the absence of STX, the T_m of the aptamer is about 69.8 °C. Such a high temperature suggests that the folded structure formed by duplex and G-quadruplex structure is stable under such conditions. The addition of STX decreases the value of T_m which is contrary to our general belief that the interaction between STX and aptamer could stabilize the secondary structure and increase the value of T_m. We infer that the reason is the interaction between STX and K^+. Both STX molecules and K^+ ions

are positively charged and they all were included in the folded structure. The electrostatic repulsion between them may weaken the stabilization effect of K^+ to G-quadruplex and the interaction between STX and aptamer cannot make up the loss from the effect of K^+, and consequently decrease the value of T_m. To verify the effect of STX to G-quadruplex structure, CD-melting curves were plotted by monitoring the ellipticity at 297 nm as a function of temperature (Fig. 4B). Because G-quadruplex has a characteristic peak at 297 nm, this value change could reflect the unfolding of G-quadruplex. In the absence of STX, the T_m from CD could be found at 63.4 ^{o}C which is a little lower than that from UV-melting curve. This suggests that the G-quadruplex structure contributes to part of the aptamer conformation. After the addition of STX with the same STX to aptamer ratios as that in UV-melting curves, the curves are shifted and the values of T_m are decreased demonstrating that STX lowers the thermal stability of G-quadruplex. These observations are coincident with the conclusion obtained above.

It can be seen that all the STX-aptamer complexes are stable under low temperatures (lower than 38 ^{o}C) and it is hard to distinguish them. With the increase of temperature, the STX-aptamer complexes containing different concentrations of STX start to unfold at different extents. They were unfolded completely under high temperatures (higher than 90 ^{o}C) which are also difficult to be distinguished. The absorption difference between the solutions of the aptamer in the presence and absence of STX at different temperatures is plotted in Fig. 4C. As predicted, there is a maximum of the absorption difference which is estimated at about 61 ^{o}C. The conformation of the aptamer in the presence and absence of STX could be differentiated at maximal extent under this temperature. Thus, the working temperature of 61 ^{o}C is selected as the optimal temperature for further biosensor design.

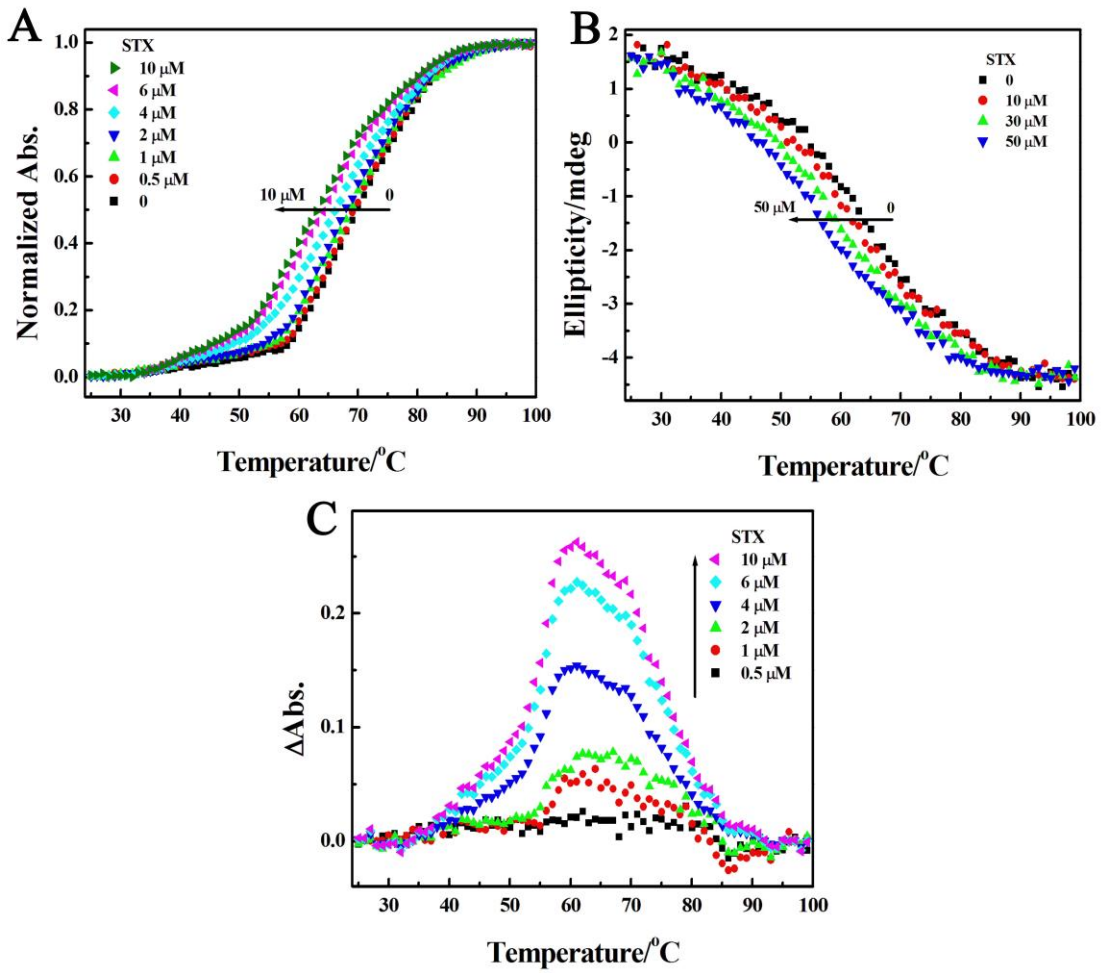

Fig. 4 (A) The UV-melting curves of the M-30f solutions (1 μM) incubated with various concentrations of STX; (B) The CD-melting curves of the M-30f solutions (5 μM) incubated with various concentrations of STX; (C) The absorption differences at 260 nm between the solutions of M-30f in the presence and absence of STX at different temperatures.

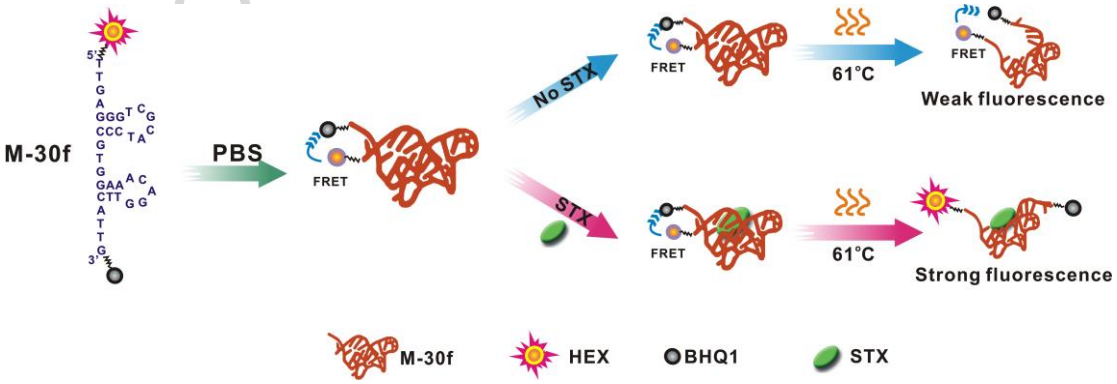

Scheme 1 Schematic illustration of the fluorescence approach for STX detection.

Aptasensor for STX detection

Then, a simple, conventional fluorescent method was designed based on the effect of STX to the conformational stability of aptamer under high temperature. As is shown in Scheme 1, the labeled aptamer (HB-M-30f) folds into a compact structure and brings the fluorophore and quencher together under low temperature. Under high temperature, the addition of STX lowers the stability of the structure and different concentrations of STX result in different unfolding extents of the structure, i.e. different FRET extents. Therefore, the concentration of STX could be reflected by the fluorescence intensity. Fig. 5A shows the fluorescent spectra of the biosensing system to increasing concentrations of STX. It can be seen that the biosening system exhibits a "turn on" response to STX. With the increase of STX concentrations, the fluorescence intensity at 553 nm increased. The intensity at 553 nm vs. STX concentrations was plotted in Fig.5B. A limit of detection (LOD) of 6.0 nM (1.8 ng/mL) (3σ) is easy to achieve. A relative standard deviation (RSD) was calculated to be 1.8% by 6 repetitive measurements of 80 nM STX, demonstrating a high accuracy and reproducibility of the assay.

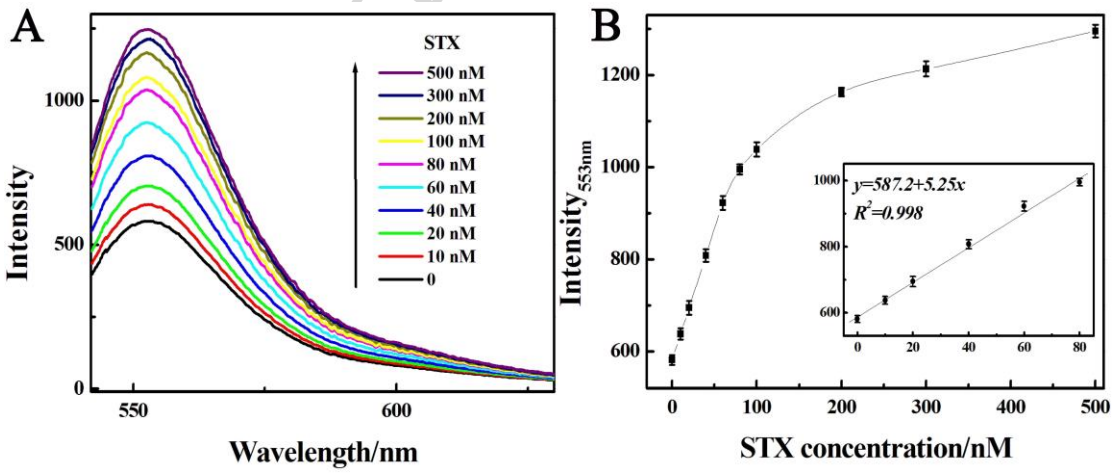

Fig. 5 Fluorescence responses of this approach toward STX: (A) changes in fluorescence spectra of the labeled aptamer (HB-M-30f, 20 nM) with increasing concentrations of STX; (B) Fluorescence intensity at 553 nm as function of concentration of STX.

To assess the selectivity of the biosensing system, control experiments were performed on some analogues of STX including water (blank) and standard solutions of GTX2&3 and NEO. The results are shown in Fig. 6. Only STX can induce the "turn-on" fluorescence response. The good selectivity is attributable to the high specificity of the aptamer for STX.

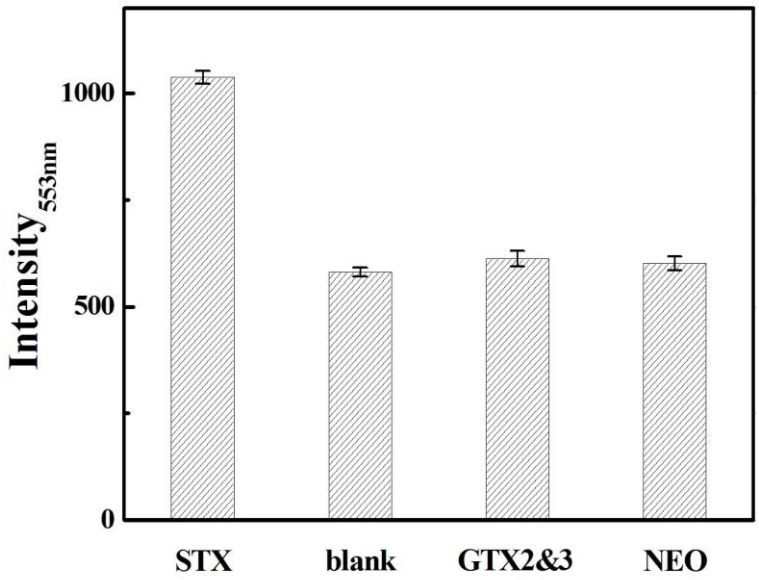

Fig. 6 Fluorescence responses of this approach at 553 nm toward STX (100 nM), blank sample, GTX2&3 (100 nM), and NEO (100 nM).

Table 1
Results of STX detection in real shellfish samples (n=5).

Sample No.	Spiked (nM)	Found (nM)					Average Recovery (%)	RSD (%)
		1	2	3	4	5		
1	20	19.8	23.4	22.5	21.9	22.8	110.4	5.6
2	50	54.3	50.5	56.1	60.0	57.2	111.2	5.7
3	80	80.1	89.2	87.7	84.3	81.5	105.7	4.1

Table 2

Comparison between several methods for STX detection.

Methods	Linear range	LOD	Operation steps	Reference
Biolayer interferometry aptasensor	100 - 800 ng/mL	0.5 ng/mL	(1) Baseline (2 min); (2) loading (5 min); (3) washing (2 min); (4) association (3 min); (5) dissociation (3 min).	[2]
Electrochemical aptasensor	0.27 - 9 ng/mL	0.11 ng/mL	(1) Preparation of SAM-modified gold electrode (24 h); (2) adsorption of MB anchored MWCNTs; (3) Carboxy groups activation (1 h) and aptamer linkage; (4) deposition of sample (30 min) and DPV measurements.	[6]
ELISA	0.020 - 0.80 ng/mL (human whole blood) 0.06 - 2.0 ng/mL (dried human blood)	0.019 ng/mL (human whole blood) 0.06 ng/mL (dried human blood)	(1) Sample drop; (2) addition of polyclonal rabbit antibody and enzyme conjugate solution (incubation 1 h with shaking); (3) contents remove and wash; (4) addition of substrate and incubation 30 min with shaking; (5) stop solution and measurement.	[1]
LC-ESI-MS/MS method	5 - 124 ng/mL	1.5 ng/mL	(1) Calibration standards preparation; (2) column equilibration; (3) LC-MS performance for standards and samples (45 min for each); (4) column re-equilibration	[5]
Fluorescent aptasensor	0 - 24 ng/mL	1.8 ng/mL	(1) Incubation (30 min); (2) measurement at 61 ºC.	This work

Application of the aptasensor in real shellfish samples

Finally, the application of the fluorescent aptasensor for the detection of STX in real samples was demonstrated. STX standard solutions were spiked into shellfish samples and extracted to achieve final concentrations of 20 nM, 50 nM, and 80 nM. The samples were analyzed using this aptasensor and the results were shown in Table 1. The recoveries were from 105.7% to 111.2% indicating a good accuracy and reproducibility of the aptasensor. The low RSD of 4.1% to 5.7% demonstrates a good repeatability

of this method. As a monitoring method for food safety, its feasibility for onsite application should be evaluated. The comparison of this fluorescent aptasensor with other detection methods is listed in Table 2. Although the LOD of our method is not the lowest, it is low enough to satisfy the standard of AOAC (maximum permitted limit of STX (3 ng/mL) in drinking water and the detection limit of HPLC (10 ng/mL)). It can be seen that the advantage of this aptasensor has the simplest operation steps with just incubation between aptamer and analyte before measurement.

Conclusion

In this work, the conformational switch of the STX aptamer (M-30f) upon STX binding was studied through the analysis of circular dichroism (CD) of the aptamer and the fluorescent spectra of the labeled aptamer under different buffer conditions. It is found that the conformation of the aptamer is determined by the buffer conditions rather than STX (10 mM phosphate buffer, 2.7 mM KCl, 137 mM NaCl, pH 7.4) and K^+ plays an important role in conformation stability. Combined with the results from the CV-based fluorescent assay that the binding of STX does not adopt an external stacking mode, we infer that the aptamer may provide an exactly suitable cave for STX which is consistent with Zheng's assumption. The results of UV-melting curves and circular dichroism-melting curves indicate that the presence of STX lowers the thermal stability of the aptamer conformation, and different concentrations of STX produce different unfolding extents of aptamer under high temperature. Then, a temperature-assisted "turn-on" fluorescent method was performed to detect STX using the principle that different concentrations of STX produces different unfolding extents of the structure under high temperature. The sensitivity, selectivity and the real sample application are satisfied demonstrating that this simple method could be an alternative for STX detection. What is more, the temperature-assistant method could provide a strategy for simple aptasensor design using aptamers that do not switch

conformation upon targets binding.

Acknowledgement

This work was founded by the National Natural Science Foundation of China (Nos. 31501576, 21504021, 51673056); the Preferential Foundation for Overseas Scholars, Ministry of Personnel of China (No. 2015LXKJZZ001); the Natural Science Foundation for the Higher Education Institutions of Anhui Province of China (KJ2015A428); Science and Technology Major Project of Anhui Province, China (No. 16030901053).

References

[1] R.E. Wharton, M.C. Feyereisen, A.L. Gonzalez, N.L. Abbott, E.I. Hamelin, R.C. Johnson, Quantification of saxitoxin in human blood by ELISA, Toxicon, 133 (2017) 110-115.
[2] S. Gao, X. Zheng, J. Wu, A biolayer interferometry-based competitive biosensor for rapid and sensitive detection of saxitoxin, Sensors and Actuators B: Chemical, 246 (2017) 169-174.
[3] K.G. Sellner, G.J. Doucette, G.J. Kirkpatrick, Harmful algal blooms: causes, impacts and detection, Journal of Industrial Microbiology and Biotechnology, 30 (2003) 383-406.
[4] W.F. Pearman, S.M. Angel, J.L. Ferry, S. Hall, Characterization of the Ag Mediated Surface-Enhanced Raman Spectroscopy of Saxitoxin, Applied Spectroscopy, 62 (2008) 727-732.
[5] C. Shin, H. Jang, H. Jo, H.-J. Kim, D.-S. Kim, J.-H. Hong, Development and validation of an accurate and sensitive LC-ESI-MS/MS method for the simultaneous determination of paralytic shellfish poisoning toxins in shellfish and tunicate, Food Control, 77 (2017) 171-178.
[6] L. Hou, L. Jiang, Y. Song, Y. Ding, J. Zhang, X. Wu, D. Tang, Amperometric aptasensor for saxitoxin using a gold electrode modified with carbon nanotubes on a self-assembled monolayer, and methylene blue as an electrochemical indicator probe, Microchimica Acta, 183 (2016) 1971-1980.
[7] D.L. Park, W.N. Adams, S.L. Graham, R.C. Jackson, Variability of mouse bioassay for determination of paralytic shellfish poisoning toxins, J. Assoc. Off. Anal. Chem., 69 (1986) 547-550.
[8] K. Campbell, L.D. Stewart, G.J. Doucette, T.L. Fodey, S.A. Haughey, N. Vilariño, K. Kawatsu, C.T. Elliott, Assessment of Specific Binding Proteins Suitable for the Detection of Paralytic Shellfish Poisons Using Optical Biosensor Technology, Analytical Chemistry, 79 (2007) 5906-5914.
[9] A.R. Humpage, V.F. Magalhaes, S.M. Froscio, Comparison of analytical tools and biological assays for detection of paralytic shellfish poisoning toxins, Analytical and Bioanalytical Chemistry, 397 (2010) 1655-1671.
[10] J.F. Lawrence, B. Niedzwiadek, C. Menard, Quantitative determination of paralytic shellfish poisoning toxins in shellfish using prechromatographic oxidation and liquid chromatography with fluorescence detection: Collaborative study, J. AOAC Int., 88 (2005) 1714-1732.
[11] A.D. Turner, R.G. Hatfield, Refinement of AOAC Official Method SM 2005.06 Liquid Chromatography-Fluorescence Detection Method to Improve Performance Characteristics for the Determination of Paralytic Shellfish Toxins in King and Queen Scallops, J. AOAC Int., 95 (2012)

129-142.

[12] W.A. Bragg, S.W. Lemire, R.M. Coleman, E.I. Hamelin, R.C. Johnson, Detection of human exposure to saxitoxin and neosaxitoxin in urine by online-solid phase extraction-liquid chromatography–tandem mass spectrometry, Toxicon, 99 (2015) 118-124.

[13] T.Y. Olson, A.M. Schwartzberg, J.L. Liu, J.Z. Zhang, Raman and Surface-Enhanced Raman Detection of Domoic Acid and Saxitoxin, Applied Spectroscopy, 65 (2011) 159-164.

[14] P. Kele, J. Orbulescu, R.E. Gawley, R.M. Leblanc, Spectroscopic detection of Saxitoxin: an alternative to mouse bioassay, Chemical Communications, (2006) 1494-1496.

[15] I. Bazin, S.A. Tria, A. Hayat, J.-L. Marty, New biorecognition molecules in biosensors for the detection of toxins, Biosensors and Bioelectronics, 87 (2017) 285-298.

[16] R.E. Gawley, S. Pinet, C.M. Cardona, P.K. Datta, T. Ren, W.C. Guida, J. Nydick, R.M. Leblanc, Chemosensors for the Marine Toxin Saxitoxin, Journal of the American Chemical Society, 124 (2002) 13448-13453.

[17] S.A. Haughey, K. Campbell, B.J. Yakes, S.M. Prezioso, S.L. DeGrasse, K. Kawatsu, C.T. Elliott, Comparison of biosensor platforms for surface plasmon resonance based detection of paralytic shellfish toxins, Talanta, 85 (2011) 519-526.

[18] A. Szkola, E.M. Linares, S. Worbs, B.G. Dorner, R. Dietrich, E. Martlbauer, R. Niessner, M. Seidel, Rapid and simultaneous detection of ricin, staphylococcal enterotoxin B and saxitoxin by chemiluminescence-based microarray immunoassay, Analyst, 139 (2014) 5885-5892.

[19] S.D. Jayasena, Aptamers: An emerging class of molecules that rival antibodies in diagnostics, Clinical Chemistry, 45 (1999) 1628-1650.

[20] R.R. Breaker, DNA aptamers and DNA enzymes, Current Opinion in Chemical Biology, 1 (1997) 26-31.

[21] A.D. Ellington, J.W. Szostak, In vitro selection of RNA molecules that bind specific ligands, Nature, 346 (1990) 818-822.

[22] W. Zhou, P.-J. Jimmy Huang, J. Ding, J. Liu, Aptamer-based biosensors for biomedical diagnostics, Analyst, 139 (2014) 2627-2640.

[23] K. Han, Z.Q. Liang, N.D. Zhou, Design Strategies for Aptamer-Based Biosensors, Sensors-Basel, 10 (2010) 4541-4557.

[24] M. Hasanzadeh, N. Shadjou, M. de la Guardia, Aptamer-based assay of biomolecules: Recent advances in electro-analytical approach, TrAC Trends in Analytical Chemistry, 89 (2017) 119-132.

[25] H.B. Seo, M.B. Gu, Aptamer-based sandwich-type biosensors, Journal of Biological Engineering, 11 (2017) 11.

[26] K. Muzyka, M. Saqib, Z. Liu, W. Zhang, G. Xu, Progress and challenges in electrochemiluminescent aptasensors, Biosensors and Bioelectronics, 92 (2017) 241-258.

[27] F.S. Sabet, M. Hosseini, H. Khabbaz, M. Dadmehr, M.R. Ganjali, FRET-based aptamer biosensor for selective and sensitive detection of aflatoxin B1 in peanut and rice, Food Chemistry, 220 (2017) 527-532.

[28] S.M. Handy, B.J. Yakes, J.A. DeGrasse, K. Campbell, C.T. Elliott, K.M. Kanyuck, S.L. DeGrasse, First report of the use of a saxitoxin–protein conjugate to develop a DNA aptamer to a small molecule toxin, Toxicon, 61 (2013) 30-37.

[29] K. Alfaro, P. Bustos, C. O'Sullivan, P. Conejeros, Facile and Cost-Effective Detection of Saxitoxin Exploiting Aptamer Structural Switching, Food Technol. Biotechnol., 53 (2015) 337-341.

[30] X. Zheng, B. Hu, S.X. Gao, D.J. Liu, M.J. Sun, B.H. Jiao, L.H. Wang, A saxitoxin-binding

aptamer with higher affinity and inhibitory activity optimized by rational site-directed mutagenesis and truncation, Toxicon, 101 (2015) 41-47.

[31] M. Naderi, M. Hosseini, M.R. Ganjali, Naked-eye detection of potassium ions in a novel gold nanoparticle aggregation-based aptasensor, Spectrochimica Acta Part A: Molecular and Biomolecular Spectroscopy, 195 (2018) 75-83.

[32] Y. Guo, Y. Chen, Y. Wei, H. Li, C. Dong, Label-free fluorescent aptasensor for potassium ion using structure-switching aptamers and berberine, Spectrochimica Acta Part A: Molecular and Biomolecular Spectroscopy, 136 (2015) 1635-1641.

[33] F. Salehnia, M. Hosseini, M.R. Ganjali, A fluorometric aptamer based assay for cytochrome C using fluorescent graphitic carbon nitride nanosheets, Microchimica Acta, 184 (2017) 2157-2163.

[34] Y.-S. Borghei, M. Hosseini, M.R. Ganjali, S. Hosseinkhani, A novel BRCA1 gene deletion detection in human breast carcinoma MCF-7 cells through FRET between quantum dots and silver nanoclusters, Journal of Pharmaceutical and Biomedical Analysis, 152 (2018) 81-88.

[35] J.-H. Guo, L.-N. Zhu, D.-M. Kong, H.-X. Shen, Triphenylmethane dyes as fluorescent probes for G-quadruplex recognition, Talanta, 80 (2009) 607-613.

[36] D.-M. Kong, Y.-E. Ma, J. Wu, H.-X. Shen, Discrimination of G-Quadruplexes from Duplex and Single-Stranded DNAs with Fluorescence and Energy-Transfer Fluorescence Spectra of Crystal Violet, Chemistry – A European Journal, 15 (2009) 901-909.

[37] W. Liu, B. Zheng, S. Cheng, Y. Fu, W. Li, T.-C. Lau, H. Liang, G-quadruplex formation and sequence effect on the assembly of G-rich oligonucleotides induced by Pb^{2+} ions, Soft Matter, 8 (2012) 7017-7023.

[38] J.F. Lawrence, B. Niedzwiadek, C. Menard, Quantitative determination of paralytic shellfish poisoning toxins in shellfish using prechromatographic oxidation and liquid chromatography with fluorescence detection: Interlaboratory study, J. AOAC Int., 87 (2004) 83-100.

[39] M. Vorlíčková, I. Kejnovská, K. Bednářová, D. Renčiuk, J. Kypr, Circular Dichroism Spectroscopy of DNA: From Duplexes to Quadruplexes, Chirality, 24 (2012) 691-698.

Figure captions

Fig. 1 (A) CD spectra of M-30f (5 μM) under various buffer conditions: 1) PBS buffer (10 mM phosphate buffer, 2.7 mM KCl, 137 mM NaCl, pH 7.4), 2) the addition of 5 μM STX under PBS condition, 3) the addition of 10 μM STX under PBS condition, 4) Tris-HCl buffer (10 mM Tris-HCl, pH 7.4) with 2.7 mM KCl, and 5) Tris-HCl buffer; (B) The obtained CD spectra by subtracting Line 5 from Line 1-4 in (A).

Fig. 2 (A) Fluorescence spectra of HB-M-30f (100 nM) in the presence of various concentrations of STX in PBS buffer and Tris-HCl buffer (solid lines), and fluorescence spectrum of HB-M-30f (100 nM) in pure PBS buffer (dotted line). (B) Fluorescence spectra of HB-M-30f (100 nM) in the presence of various concentrations of K^+ in pure PBS buffer. The inset is the fluorescence intensity at 553 nm as function of concentration of K^+. The chemical structures of HEX and BHQ1 are shown at the bottom of this figure.

Fig. 3 Fluorescence spectrum of CV (8 μM) (Line 1), and spectra of the mixture of CV (8 μM) and M-30f (4 μM) in the presence of various concentrations of STX (Line 2: 0 STX; Line 3: 4 μM STX; Line 4: 8 μM STX).

Fig. 4 (A) The UV-melting curves of the M-30f solutions (1 μM) incubated with various concentrations of STX; (B) The CD-melting curves of the M-30f solutions (5 μM) incubated with various concentrations of STX; (C) The absorption differences at 260 nm between the solutions of M-30f in the presence and absence of STX at different temperatures.

Scheme 1 Schematic illustration of the fluorescence approach for STX detection.

Fig. 5 Fluorescence responses of this approach toward STX: (A) changes in fluorescence spectra of the labeled aptamer (HB-M-30f, 20 nM) with increasing concentrations of STX; (B) Fluorescence intensity

at 553 nm as function of concentration of STX.

Fig. 6 Fluorescence responses of this approach at 553 nm toward STX (100 nM), blank sample, GTX2&3 (100 nM), and NEO (100 nM).

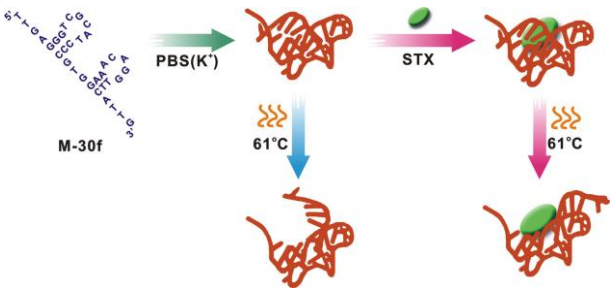

Graphical abstract

Highlights

- The conformation of the aptamer (M-30f) is determined by the buffer conditions rather than saxitoxin (STX).
- K^+ ions could induce the aptamer to fold into a more compact conformation which involves duplex and G-quadruplex structures.
- The formation of duplex and G-quadruplex structure may provide an exactly suitable cave for STX binding.
- A simple temperature-assisted "turn-on" fluorescent method was performed to detect STX.